

## X-ray-scattering study of the two magnetic correlation lengths in uranium antimonide

S. C. Perry, W. J. Nuttall,\* and W. G. Stirling†

Physics Department, School of Physical Science and Engineering, Keele University, Staffordshire, ST5 5BG, United Kingdom

G. H. Lander

European Commission, Joint Research Centre, Institute for Transuranium Elements, Postfach 2340, D-76125 Karlsruhe, Federal Republic of Germany

O. Vogt

Laboratorium für Festkörperphysik, Eidgenössische Technische Hochschule Zürich, CH-8093 Zürich, Switzerland

(Received 5 October 1995; revised manuscript received 19 August 1996)

In common with some other recent critical scattering studies we have observed the presence of a second component in the critical fluctuations close to the continuous magnetic phase transition in USb. It is found that the magnetic anisotropy of this second component does not exhibit the same directional dependence as the ‘normal’ critical scattering and that the critical behavior of this feature is not consistent with an Ornstein-Zernike treatment of the scaling. [S0163-1829(96)05645-7]

The existence of a second length scale in the critical fluctuations close to magnetic phase transitions has been observed in a number of systems<sup>1-3</sup> (these results are similar to the earlier two-length-scale observations of the structural transitions in perovskites<sup>4-6</sup>). The basis for this view is that the wave vector dependence of the scattered intensity may be best described by a *two-component* line shape consisting of a broad function added to another much sharper function. This suggests that the fluctuations in the order of the system are occurring on length scales up to two *different* maxima. We have observed similar ‘two-component’ line shapes in the critical scattering from uranium antimonide.

Type-I antiferromagnets with the single- $\mathbf{q}$  structure in which the direction of the propagation vector is parallel to the ordered magnetic moment are expected to belong to the  $n=3$  universality class.<sup>7</sup> A similar analysis leads to the same conclusion for USb,<sup>8</sup> which has the triple- $\mathbf{q}$  structure (although the critical scattering from the single- and triple- $\mathbf{q}$  arrangements is identical.<sup>9</sup>) Brézin *et al.*<sup>10</sup> have shown that for values of  $n \leq 3$  the critical properties of a system should be independent of anisotropy in the Hamiltonian, and should depend only on  $n$  and the spatial dimensionality. We expect the USb system to display the critical properties of the three-dimensional (3D) Heisenberg universality class. The crystal structure of USb is face centered cubic (fcc), and below the Néel temperature ( $T_N \sim 200$  K) the ordering wave vector points along one of the three principle axes, so that magnetic peaks are visible at positions of systematic absences of the fcc structure. The critical scattering exhibits a large degree of directional anisotropy as the exchange coupling is stronger within the (0,0,1)-type sheets of spins ( $J_{\perp}$ ) than it is between them ( $J_{\parallel}$ ). In this paper we present measurements of the critical exponents and anisotropy for the USb system at the (0,0,3) and  $(\bar{1},0,2)$  positions.

Two experiments were performed under similar conditions at beam line X22C of the National Synchrotron Light Source (NSLS) at Brookhaven National Laboratory, using the same sample. No special surface treatments were per-

formed. The technique of x-ray resonant exchange scattering (XRES) was used to maximize the magnetic signal by tuning the incident x-ray energy close to that of the uranium  $M_{IV}$  absorption edge (3.728 keV).<sup>11</sup> The USb sample measured  $\sim 4 \times 2 \times 1.5$  mm and the full width at half maximum (FWHM) of the rocking curve measured at 3.728 keV was  $0.05^\circ$ . The absorption limited penetration depth at this energy depends upon the geometry, but is of the order of 1500 Å. The crystal was mounted with the  $c$  face upward such that the  $\langle H,0,L \rangle$  directions spanned the scattering plane, and was contained within a closed-cycle refrigerator capable of cool-

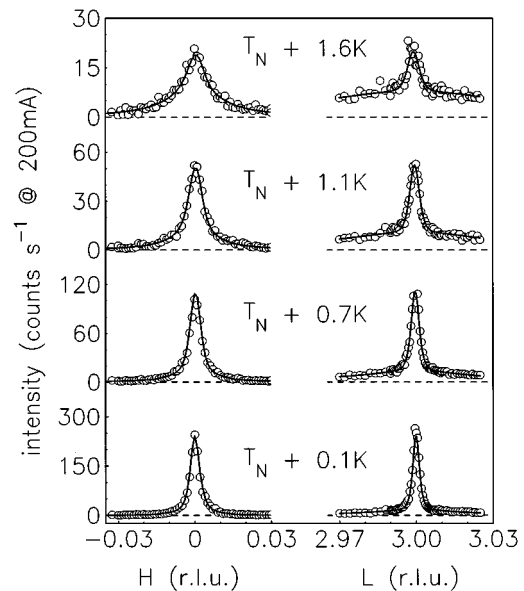


FIG. 1. Center regions of scans in the  $H$  and  $L$  directions at the (0,0,3) position at various temperatures. A high-temperature background has been subtracted from the data; therefore all the intensity above the dashed line is critical scattering. The solid lines are fits described in the text.

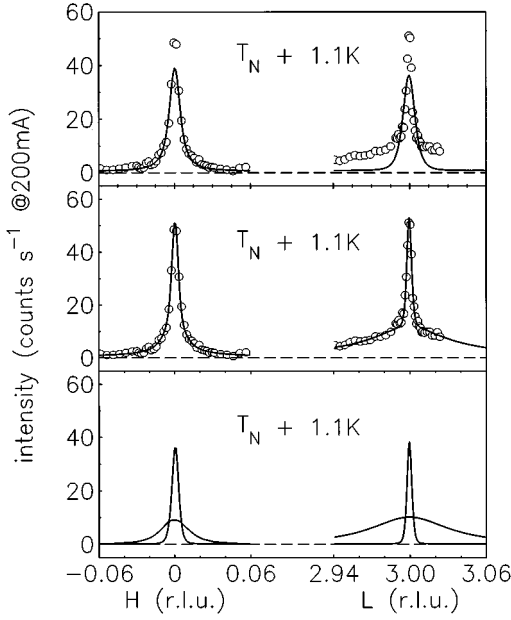


FIG. 2. Comparison of fitting functions: the upper panel shows the best fit obtainable with a scattering function of pure Lorentzian character, and the middle panel shows the best fit with a scattering function which is the sum of Lorentzian and squared-Lorentzian components. The solid lines in the lower panel show the separate components of the fit. Geometrical constraints of the diffractometer prevented us from measuring at scattering vectors of greater magnitude than 3.03 reciprocal lattice units (r.l.u.) at the uranium  $M_{IV}$  edge energy.

ing down to 12 K, with temperature stability  $\pm 0.01$  K at 200 K.

$T_N$  was determined by measuring the integrated intensity of the magnetic scattering as a function of reduced temperature. The dominant contribution to the resonant dipole cross section is proportional to the two-spin correlation function (as in neutron diffraction),<sup>12</sup> hence the magnetic intensity may be described by the power law  $I(t) \sim |t|^{2\beta}$ . The transition temperature was found to be  $202.2 \pm 0.1$  K, with  $\beta = 0.36 \pm 0.03$ , in agreement with the value from the 3D Heisenberg model<sup>13</sup> of  $\beta = 0.367$ .

Measurements of the critical scattering above  $T_N$  at the  $(0,0,3)$  and  $(\bar{1},0,2)$  positions have been made with reciprocal-space scans in the  $H$  and  $L$  directions. Examples of the data are shown in Fig. 1. The conventional form for the pair correlation is  $G(r) \sim r^{-(1+\eta)} \exp(-r/\xi)$ ; the Ornstein-Zernike (OZ) approximation corresponds to  $\eta=0$  and Fourier transforms in 3D to give a Lorentzian structure factor. As with previous studies,<sup>3</sup> the structure factor we have found to provide the best description of the data is the sum of a Lorentzian ( $\mathcal{L}$ ) and a squared-Lorentzian ( $\mathcal{L}2$ ) function,

$$S(\mathbf{q}) = \frac{\chi_0}{1 + [(q_{\parallel} - q_{\parallel 0})/\kappa_{\parallel}]^2 + [(q_{\perp} - q_{\perp 0})/\kappa_{\perp}]^2} + \frac{\chi'_0}{\{1 + [(q_{\parallel} - q_{\parallel 0})/\kappa'_{\parallel}]^2 + [(q_{\perp} - q_{\perp 0})/\kappa'_{\perp}]^2\}^2}. \quad (1)$$

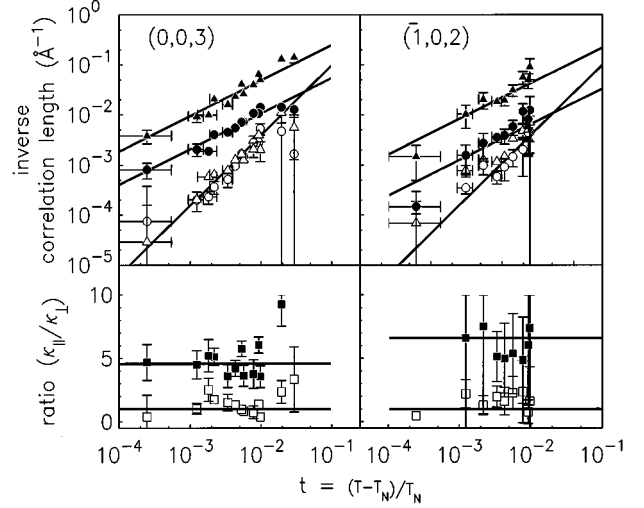


FIG. 3. Upper panels: inverse correlation lengths in the directions parallel (triangles) and perpendicular (circles) to the propagation direction as a function of reduced temperature for the  $(0,0,3)$  (left-hand side) and  $(\bar{1},0,2)$  (right-hand side) positions. The solid symbols represent values for the broad component and the open symbols represent values for the narrow component. The solid lines through the broad component values show the 3D Heisenberg value for  $\nu$  of 0.71. The solid lines through the narrow component values have  $\nu'$  fixed at 1.3. Lower panels: anisotropy ratio (squares) of the parallel to the perpendicular components for the data points shown directly above.

We follow the convention of representing narrow component values by primed ( $'$ ) letters. The solid lines in Fig. 1 and in the middle panel of Fig. 2 show the best fit of the above function convoluted with the instrumental resolution. In these fits the  $\mathcal{L}2$  component has much smaller widths ( $\kappa'_{\parallel}$  and  $\kappa'_{\perp}$ ) than the  $\mathcal{L}$  component; hence the  $\mathcal{L}2$  function is considered to represent the “narrow” component and the  $\mathcal{L}$  function the “broad” component. Although we do not suggest that the  $\mathcal{L} + \mathcal{L}2$  combination is a *unique* representation of the data, this model appears to be a very good description. A single-component structure factor is not a satisfactory description of the observed scattering, as shown in the top panel of Fig. 2.

Critical scattering at the  $(0,0,3)$  position was visible at 10 K above the transition temperature, although the two component nature of the scans is visible only up to  $\sim T_N + 2$  K. At this position we present data at 13 temperatures from  $T_N + 0.05$  K to  $T_N + 6$  K. The magnetic structure factor is

TABLE I. Values of  $\nu$  and  $\nu'$  exponents, compared with previous results obtained from neutron- and x-ray-scattering measurements.

	$(0,0,3)$	$(\bar{1},0,2)$	Previous
$\nu_{\parallel}$	$0.88 \pm 0.07$	$0.90 \pm 0.15$	$0.66 \pm 0.05^8$
$\nu_{\perp}$	$0.70 \pm 0.07$	$1.00 \pm 0.15$	$0.72 \pm 0.04^8$
$\nu'_{\parallel}$	$1.09 \pm 0.25$	$1.2 \pm 0.3$	$0.90 \rightarrow 1.30^{1-3}$
$\nu'_{\perp}$	$1.44 \pm 0.06$	$1.8 \pm 0.3$	

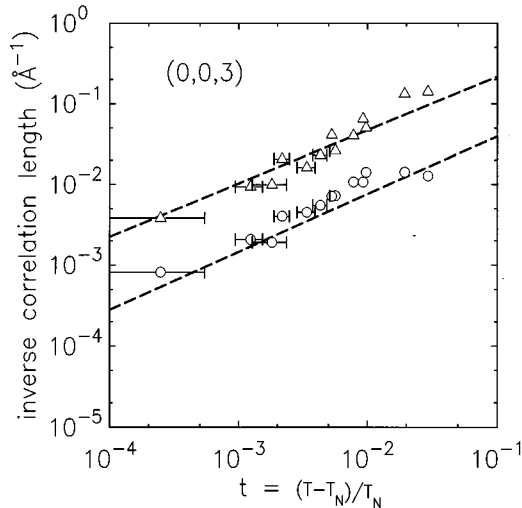


FIG. 4. Comparison of the broad component inverse correlation lengths of the (0,0,3) critical scattering (triangles,  $\kappa_{\parallel}$ ; circles,  $\kappa_{\perp}$ ) with the power-law fits to neutron data of Hagen *et al.* (Ref. 8) (dashed lines).

such that the scattering at the  $(\bar{1},0,2)$  position is weaker than at (0,0,3); hence the statistical quality of our data at  $(\bar{1},0,2)$  is poorer, and at this position we have useful data at nine temperatures ranging from  $T_N + 0.05$  K to  $T_N + 2$  K.

The temperature dependence of the broad component width, as extracted from best fits of the type mentioned above, is shown in Fig. 3 with solid symbols. The data have been fitted to separate power law functions,  $\kappa \sim t^{\nu}$ , for the parallel and perpendicular components at the two positions. The value of  $T_N$  used in these fits was constrained to the value determined by the order parameter measurement; this agrees (within error) with the values obtained if  $T_N$  is allowed to vary. The results are presented in Table I. As demonstrated in Fig. 3, these results are consistent with the 3D Heisenberg value ( $\nu = 0.71$ ); the slightly higher than expected freely fitted values appear to be caused by temperature uncertainties at very small reduced temperatures and by low intensity at larger reduced temperatures. With the exponent fixed, the anisotropy measured by the ratio of the two functions is  $4.6 \pm 0.6$  for the (0,0,3) data, and  $6.6 \pm 1.5$  for the  $(\bar{1},0,2)$  data, as shown in the lower panels of Fig. 3. These results are in excellent agreement with the previous neutron scattering measurement of  $4.9 \pm 0.7$ ,<sup>8</sup> as are the absolute values of the inverse correlation lengths, shown in Fig. 4.

The temperature dependence of the narrow component width has been analyzed in a similar fashion; the data are shown in Fig. 3 as open symbols and the results of the power law fits are presented in Table I. The solid lines in the upper panels of Fig. 3 show fits with  $\nu'$  fixed at 1.3, which is a good average description of the data. In contrast to the results of the broad component fits, we find it difficult to resolve the anisotropy in the narrow component; power law fits with  $\nu'$  fixed at 1.3 give ratios of  $0.8 \pm 0.1$  for (0,0,3) and  $1.4 \pm 0.2$  for  $(\bar{1},0,2)$  data. This is demonstrated in the lower

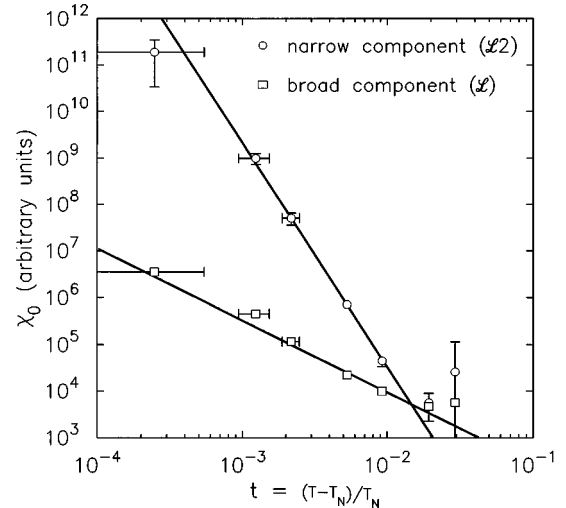


FIG. 5. Static susceptibility values as a function of reduced temperature for the (0,0,3) data from the second experiment. The solid lines are fits to the function  $\chi_0 = At^{-\gamma}$ , as discussed in the text. The data at the highest temperature shown were not included in the fits.

panel of Fig. 3 (the lower solid lines show unity). We believe that this result may be significant in the explanation of the narrow component scattering.

The amplitudes of the scattering functions  $\chi_0$  and  $\chi'_0$  have been extracted from fits of the best data [the (0,0,3) position during the second experiment] and are plotted in Fig. 5. The rapid decay of the narrow component above  $T_N$  is clearly illustrated. The solid lines are fits to the power law,  $\chi_0 = At^{-\gamma}$ , and the results are  $\gamma = 1.54 \pm 0.14$  and  $\gamma' = 4.8 \pm 1.3$ . The 3D Heisenberg value<sup>13</sup> for  $\gamma$  is 1.4. Large values for the  $\gamma'$  exponent have been reported for other systems, such as NpAs.<sup>3</sup> In particular, for holmium, Thurston *et al.*<sup>1</sup> report values between 2 and 5, depending on the transition temperature used in the fitting procedure.

The Fisher modification to the OZ approximation gives the definition of the  $\eta$  exponent,  $S(q)|_{T=T_c} \sim 1/(q^{2-\eta})$ . Fisher also proposes that

$$S(q)|_{T \neq T_c} \sim \frac{1}{(\kappa^2 + q^2)^{1-\eta/2}}, \quad (2)$$

and based on the need for analyticity at the transition this gives the relation  $\gamma = (2 - \eta)\nu$ . The calculated value of  $\eta$  for the 3D Heisenberg universality class is 0.037, which is consistent with our data for the broad component. However, for the narrow component we have, using  $\gamma'$  and the average value of  $\nu'$  for the (003) data,  $\eta' = -1.7 \pm 0.9$ , which clearly excludes the 3D Heisenberg value.

In conclusion, we are able to state that the critical behavior of the second component is *not* consistent with the usual treatment of 3D magnetic phase transitions; the error margin for the  $\eta'$  exponent lies outside the predictions for both the OZ approximation and the 3D Heisenberg model. This implies that the form of the correlation function is significantly

altered from that of the “normal” critical scattering. Further work, both experimental and theoretical, will be required before a comprehensive understanding of this phenomenon is obtained.

#### ACKNOWLEDGMENTS

The authors wish to thank M. E. Hagen, M. Altarelli, R. J. Birgeneau, and S. Langridge for useful advice and discus-

sions. We appreciate the help of G. Watson, D. Gibbs, W. Schoenig, and D. S. Coburn during the experiments at X22C. S.C.P., W.J.N., and W.G.S. are grateful to the UK Engineering and Physical Sciences Research Council for financial assistance. The support of the European Community SCIENCE and Human Capital Mobility programmes is acknowledged. The National Synchrotron Light Source is supported by the U.S. Department of Energy under Contract No. DE-AC02-76CH00016.

\*Present address: School of Physics and Space Research, University of Birmingham, B15 2TT, UK.

†Present address: Department of Physics, Oliver Lodge Laboratory, University of Liverpool, L69 3BX, UK.

<sup>1</sup>T. R. Thurston, G. Helgesen, J. P. Hill, D. Gibbs, B. D. Gaulin, and P. J. Simpson, *Phys. Rev. B* **49**, 15 730 (1994).

<sup>2</sup>K. Hirota, G. Shirane, P. M. Gehring, and C. F. Majkrzak, *Phys. Rev. B* **49**, 11 967 (1994).

<sup>3</sup>S. Langridge, W. G. Stirling, G. H. Lander, and J. Rebizant, *Phys. Rev. B* **49**, 12 022 (1994).

<sup>4</sup>A. Gibaud, R. A. Cowley, and P. W. Mitchell, *J. Phys. C* **44**, 2437 (1991).

<sup>5</sup>D. F. McMorrow, N. Hamaya, S. Shimomura, Y. Fujii, S. Kishimoto, and H. Iwasaki, *Solid State Commun.* **76**, 443 (1990).

<sup>6</sup>A. Gibaud, H. You, S. M. Shapiro, and J. Y. Gesland, *Phys. Rev. B* **44**, 2437 (1991).

<sup>7</sup>D. Mukamel and S. Krinsky, *Phys. Rev. B* **13**, 5065 (1976).

<sup>8</sup>M. Hagen, W. G. Stirling, and G. H. Lander, *Phys. Rev. B* **37**, 1846 (1988).

<sup>9</sup>W. J. L. Buyers and T. M. Holden, in *Handbook on the Physics and Chemistry of the Actinides*, edited by A. J. Freeman and G. H. Lander (North-Holland, Amsterdam, 1985), Vol. 2, Chap. 4.

<sup>10</sup>E. Brézin, J. C. L. Guillou, and J. Zinn-Justin, *Phys. Rev. B* **10**, 892 (1974).

<sup>11</sup>W. G. Stirling and G. H. Lander, *J. Appl. Phys.* **73**, 6877 (1993).

<sup>12</sup>J. Luo, G. T. Trammell, and J. P. Hannon, *Phys. Rev. Lett.* **71**, 287 (1993).

<sup>13</sup>M. F. Collins, *Magnetic Critical Scattering* (Oxford University Press, Oxford, 1989).